arXiv:1106.6108v2 [nucl-th] 28 Dec 2011

Pion productions by proton and Helium-3 on ^{197}Au target at beam energies of 2.8, 5, 10 and 16.587 GeV/nucleon

Gao-Chan Yong, Xurong Chen, Hu-Shan Xu, and Wei Zuo
Institute of Modern Physics, Chinese Academy of Sciences, Lanzhou 730000, China

Based on a Relativistic Boltzmann-Uehling- Uhlenbeck transport model, proton and ^{3}He induced reactions on ^{197}Au target at beam energies of 2.8, 5, 10 and 16.587 GeV/nucleon are studied. It is found that compared with proton induced reactions, ^{3}He induced reactions give larger cross sections of pion production, about 5 times those of the proton induced reactions. And more importantly, pion production from ^{3}He induced reaction is more inclined to low-angle emission. Neutrino production via positively charged pion is also discussed accordingly.

PACS numbers: 24.10.Jv, 25.40.-h, 25.55.-e, 24.10.Lx

There exists considerable interest in the possibility that one type of neutrino may transform into another type while propagation [1]. It was also argued that neutrino oscillations are related to stellar collapse [2] and spontaneous parity non-conservation [3]. Nowadays atmospheric [4–6], reactor [7], solar neutrino [8, 9] and accelerator neutrinos [10] provide compelling evidences for neutrino mass and oscillation. It is interesting to note that the precise neutrino oscillation parameters are determined by the KamLAND [11] recently. For more about neutrino physics, please see Ref. [12]. In the accelerator based neutrino experiments, a key issue toward the development of a muon collider or neutrino beam based on a muon storage ring is the design of a target/capture system capable of capturing a large number of pions. These pions then proceed into a decay channel where the resultant muon decay products are harvested before being conducted into a cooling channel and then subsequently accelerated to the final energy of the facility [13]. Understanding of the production of pions in proton interactions with nuclear targets is thus essential for determining the flux of neutrinos in accelerator based neutrino experiments [14, 15]. A large amount of data were collected by the HARP Collaboration experiments for the above physical subjects recently [16]. In fact, in accelerator based neutrino experiments, some times one needs Helium-3 induced reaction. There are many simulation methods focus on such studies, such as the phenomenological Monte Carlo generators GEANT4 [17] and MARS [18] and other theoretical works that considering more physical processes [19–25]. In this article, after checking the reliability a relativistic transport model (ART) we made comparative studies of pion production in proton and ^{3}He induced reactions on ^{197}Au target at incident beam energies of 2.8, 5, 10 and 16.587 GeV/nucleon. And finally, we simply discussed neutrino production via positively charged pion.

The well-known Boltzmann-Uehling-Uhlenbeck (BUU) model [26] has been very successful in studying heavy-ion collisions at intermediate energies. The ART (A Relativistic Transport) model [27] is the relativistic form of the BUU model, in order to simulate heavy-ion collisions at higher energies, some new physics were added. It includes baryon-baryon, baryon-meson, and meson-meson elastic and inelastic scatterings. The ART model includes the following baryons N, $\Delta(1232)$, $N^*(1440)$, $N^*(1535)$, Λ, Σ, and mesons π, ρ, ω, η, K, as well as their explicit isospin degrees of freedom. Both elastic and inelastic collisions among most of these particles are included. For baryon-baryon scatterings, the ART model includes the following inelastic channels: $NN \leftrightarrow N(\Delta N^*)$, $NN \leftrightarrow \Delta(\Delta N^*(1440))$, $NN \leftrightarrow NN(\pi\rho\omega)$, $(N\Delta)\Delta \leftrightarrow NN^*$, and $\Delta N^*(1440) \leftrightarrow NN^*(1535)$. In the above, N^* denotes either $N^*(1440)$ or $N^*(1535)$, and the symbol (ΔN^*) denotes a Δ or an N^*. For meson-baryon scatterings, the ART model includes the following reaction channels for the formation and decay of resonances: $\pi N \leftrightarrow (\Delta N^*(1440)\ N^*(1535))$, and $\eta N \leftrightarrow N^*(1535)$. There are also elastic scatterings such as $(\pi\rho)(N\Delta N^*) \to (\pi\rho)(N\Delta N^*)$. For meson-meson interactions, the ART model includes both elastic and inelastic $\pi\pi$ interactions, with the elastic cross section consisting of ρ meson formation and the remaining part treated as elastic scattering. Also included are reaction channels relevant to kaon production. The extended ART model is one part of AMPT (A Multi-Phase Transport Model) model [28]. We use the Skyrme-type parametrization for the mean field which reads [27]

$$U(\rho) = A(\rho/\rho_0) + B(\rho/\rho_0)^\sigma. \tag{1}$$

Where $\sigma = 7/6$, A = -0.356 MeV is attractive and B = 0.303 MeV is repulsive. With these choices, the ground-state compressibility coefficient of nuclear matter K=201 MeV. More details of the model can be found in the original Ref. [27].

To check the reliability of using the ART model to study the cross sections of pion production in proton or ^{3}He induced reactions, we first made a comparison of pion production in p+Au reaction at an incident beam momentum of 17.5 GeV/c between the theoretical simulations and the E910 data [14] as shown in Fig. 1. The top panel of Fig. 1 shows the inclusive differential cross sections of pion production from p+Au at an incident beam momentum of 17.5 GeV/c. We can see that for both π^- and π^+, our results fit the E910 data very well, especially at higher momenta. Pion production of p+Cu reaction

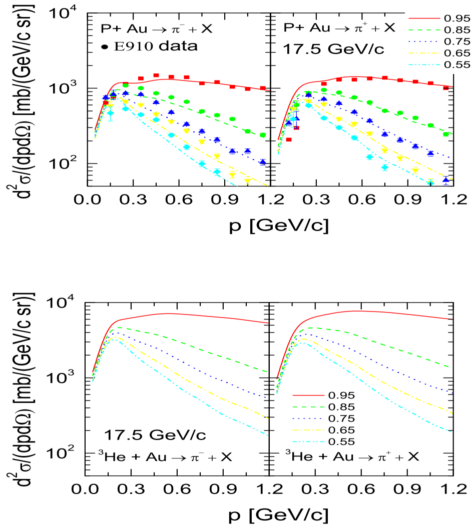

FIG. 1: (Color online) Top: Production cross sections of π^-(left column) and π^+(right column) from p+Au at the incident beam momentum of 17.5 GeV/c ($E_{beam} \sim 16.587$ GeV/nucleon) shown in bins of $\cos\theta$ (relative to beam direction). Numbers in the legend refer to the center of each bin. Data are taken from Ref. [14]. Bottom: Same as p+Au case, but for ^{3}He+Au.

at incident beam momenta of 12.3 and 17.5 GeV/c also fit the E910 data [14] very well. From Fig. 1, we can also see that the cross sections at low-angle ($0.9 < cos\theta < 1$) are evidently larger than those at high-angles, especially for energetic pion mesons. As a comparison, we also give the case of ^{3}He+Au at the incident beam momentum of 17.5 GeV/c as shown in the bottom panel of Fig. 1. From the bottom panel of Fig. 1, it is seen that differential cross sections of pion production of the ^{3}He induced reaction are about 5 times those of the proton induced reaction at the incident beam momentum of 17.5 GeV/c. The cross sections at low-angle ($0.9 < cos\theta < 1$) are also much larger than those at high-angles.

To make comparisons systematically between p+Au and ^{3}He+Au at different incident beam energies, we plot Fig. 2-4. From the top panels of Fig. 2-4, we can clearly see that as incident beam energy decreases, cross sections of pion production of p+Au also decrease. This is understandable since pion production mainly comes from decays of resonances and energetic nucleon-nucleon collisions give more resonances. We can also see that as beam energy decreases, the energetic pion mesons also decrease rapidly. The bottom panels of Fig. 2-4 are the cases of ^{3}He+Au at different incident beam energies. Also it is seen that as beam energy decreases, differential cross sections of pion production decrease rapidly, especially for energetic pion mesons. Compared with p+Au, as the increase of incident beam energy, cross sections of pion production at low-angle of ^{3}He+Au increase more rapidly, especially for energetic pion mesons.

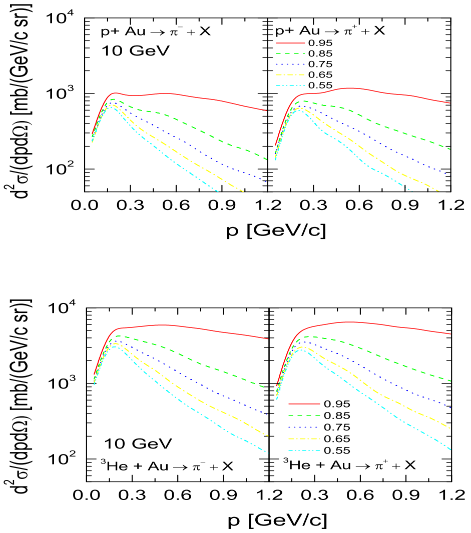

FIG. 2: (Color online) Top: Production cross sections of π^-(left column) and π^+(right column) from p+Au at the incident beam energy of 10 GeV/nucleon shown in bins of $\cos\theta$. Numbers in the legend refer to the center of each bin. Bottom: Same as p+Au case, but for ^{3}He+Au.

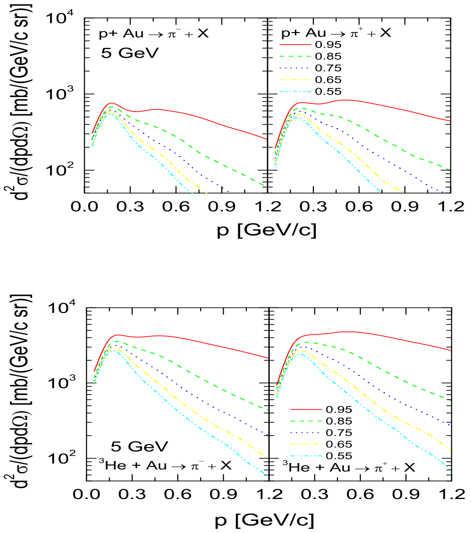

FIG. 3: (Color online) Top: Production cross sections of π^-(left column) and π^+(right column) from p+Au at the incident beam energy of 5 GeV/nucleon shown in bins of $\cos\theta$. Numbers in the legend refer to the center of each bin. Bottom: Same as p+Au case, but for ^{3}He+Au.

In the incident beam energy region from 2.8 to 16.587 GeV/nucleon, cross sections of pion production at low-angle ($0.9 < cos\theta < 1$) and high momentum of ^{3}He+Au are 5∼10 times those of p+Au case. Using the AMPT model we also made simulations for p+Au at incident beam energies from 50 to 100 GeV/nucleon, cross sec-

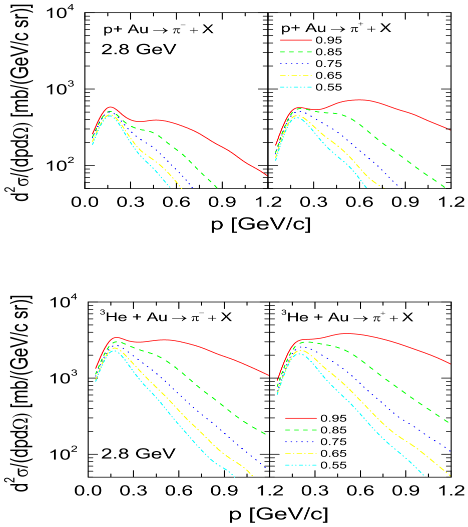

FIG. 4: (Color online) Top: Production cross sections of π^-(left column) and π^+(right column) from p+Au at the incident beam energy of 2.8 GeV/nucleon shown in bins of $\cos\theta$. Numbers in the legend refer to the center of each bin. Bottom: Same as p+Au case, but for ^{3}He+Au.

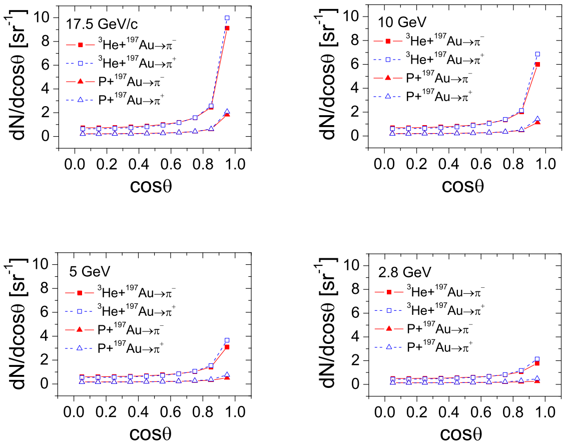

FIG. 5: (Color online) Angle distributions of pion multiplicity of p+Au and ^{3}He+Au at different incident beam energies, in bins of $\cos\theta$.

tions of pion production at low-angle ($0.9 < cos\theta < 1$) are both about 20 times those of p+Au at incident beam energy of 16.587 GeV/nucleon, indicating the saturation of cross section of pion production at the beam energy of about 50 GeV/nucleon.

We next turn to the study of angle distributions of pion multiplicity of p+Au and ^{3}He+Au at different incident beam energies. From Fig. 5, we can see that whether for p+Au or ^{3}He+Au, pion emission at low-angle increases rapidly, especially at higher incident beam energies. From these plots, we can also see that the low-

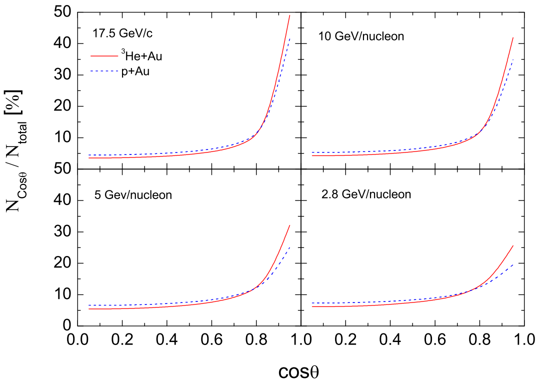

FIG. 6: (Color online) Angle distributions of charged pion relative multiplicity ($N_{cos\theta}/N_{total}$) for p+Au and ^{3}He+Au reactions at different incident beam energies, in bins of $\cos\theta$.

angle's pion emission is more pronounced for ^{3}He+Au than p+Au, especially at higher incident beam energies. Pion numbers from ^{3}He+Au at low-angle ($0.9 < cos\theta < 1$) are about 5 times those of p+Au. This indicates that ^{3}He+Au at high incident beam energy is more suitable for neutrino experiments compared with p+Au. Fig. 6 shows angle distributions of pion relative emitting number at different incident beam energies. It is seen that at the high incident beam momentum 17.5 GeV/c, relative emitting number at low-angle ($0.9 < cos\theta < 1$) can reach about 50% for ^{3}He+Au. While at incident beam energy 2.8 GeV/nucleon, relative emitting number at low-angle ($0.9 < cos\theta < 1$) reaches only about 25%. At the studied beam energy region, we can clearly see that the ^{3}He induced reaction on Au target causes larger proportional low-angle pion emission, especially at higher incident beam energies, about 5%∼ 10% larger than that of the proton induced reaction on Au target.

Fig. 7 shows cross sections of charged pion production of p+Au and ^{3}He+Au reactions at different incident beam energies. We can see that at the incident beam energies studied here, cross sections of pion production of ^{3}He and proton-induced reactions on target Au increase about 3 times. The cross sections of ^{3}He-induced reaction on target Au at the incident beam energy of 2.8 GeV/nucleon are larger than those of p+Au reaction at the beam energy of 16.587 GeV/nucleon. Fig. 8 shows the ratio of cross sections of charged pion production of p+Au and ^{3}He+Au reactions at different incident beam energies. We can clearly see that cross sections of charged pion production from ^{3}He induced reaction are about 5 times (larger than $A_{^3He}/A_H = 3$) those of the proton induced reaction.

Since the work focuses on the proton versus ^{3}He results, one wonders what scaling behavior with projectile nucleon number would one expect from a "standard" cascade model (without mean-field modifications)? Fig. 9

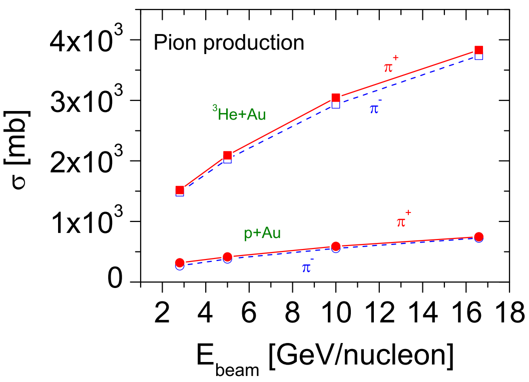

FIG. 7: (Color online) Cross sections of charged pion production of p+Au and ^{3}He+Au reactions at different incident beam energies.

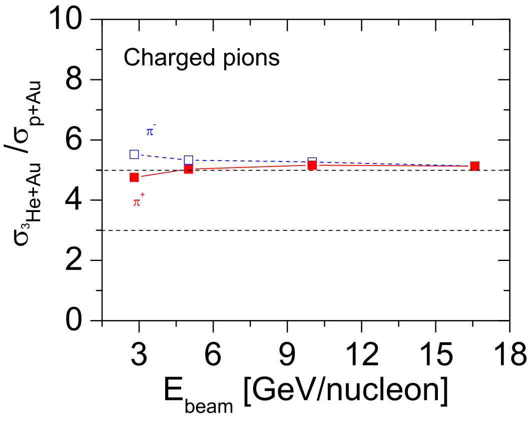

FIG. 8: (Color online) Ratio of cross sections of charged pion production of p+Au and ^{3}He+Au reactions at different incident beam energies.

shows the ratio of mean pion production per nucleon of projectile with mass number A and 1 (proton) at the incident beam energy of 2.8 GeV/nucleon (by the ART cascade model). We can see that pion production per projectile nucleon is roughly the same with different projectile mass number A, i.e., the produced total pion number is roughly proportional to projectile mass number A. This indicates each nucleon in the projectile excites pion production almost dependently. But for the projectile which mass number is smaller than the target mass number, the scaling behavior that total pion number is roughly proportional to projectile mass number A is not strictly correct. In fact, the ratio of $\frac{\pi_A}{\pi_1}/A$ is always larger than 1, as shown in Fig. 9. This is because each nucleon

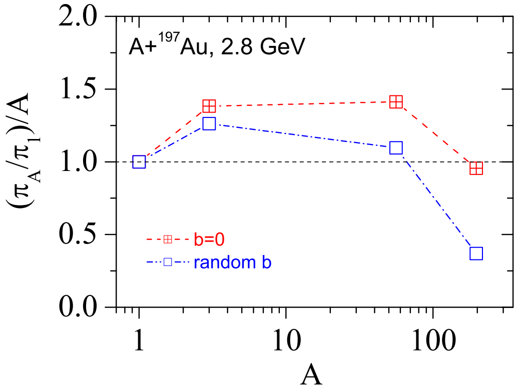

FIG. 9: (Color online) Ratio of mean pion production per nucleon of projectile with mass number A and 1 at the incident beam energy of 2.8 GeV/nucleon. The target is ^{197}Au and the impact parameters are set to be 0 and random, respectively.

in the projectile does not excite pion production independently. One nucleon in the projectile may give energy to the nucleon in the target, but does not produce pion. The other nucleon in projectile may also collide with the nucleon which has obtained energy from the other nucleon of the projectile. Thus the probability of pion production accordingly increases for the other induced nucleon in the projectile. This correlation of different incident nucleons of the projectile does not increase linearly with projectile's mass number due to the marginal collision of the induced nucleon. Thus we see about 5 times pion production of the ^{3}He induced reaction compared with the proton induced reaction. For random impact parameter case, smaller $\frac{\pi_A}{\pi_1}/A$ is due to the marginal collisions of the induced nucleon in the projectile.

To demonstrate neutrino production by proton or ^{3}He induced reactions, we plot Fig. 10, angle distributions of neutrino via π^+ decay in proton and ^{3}He induced reactions on target Au. Assuming $\pi^+ \rightarrow \mu^+ + \nu_\mu$ and pion decays into μ and ν_μ isotropically in its frame of reference, we can thus obtain neutrino distribution by assuming it rest mass 1 eV. Fig. 10 shows angle distributions of neutrino production from positively charged pion dacay in p+Au and ^{3}He+Au reactions at incident beam energies of 2.8 and 10 GeV/nucleon. We can clearly see that neutrinos from ^{3}He induced reaction are more inclined to low-angle emission than proton induced reaction, this situation is clearer for high incident beam energy. Because the energy distribution of the emitting neutrinos are important for neutrino-nucleus experiments [29–32], we also plot the energy distributions of the produced neutrinos at low and high angles as shown in Fig. 11. We can see that the produced neutrinos possess different energies from about 1 MeV to 1000 MeV and more. The most probable energy is about 30∼70 MeV for several GeV incident beam energy. Moreover, we can see that

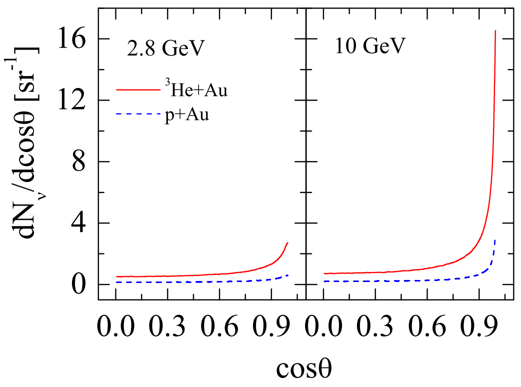

FIG. 10: (Color online) Angle distributions of neutrino production from positively charged pion decay in p+Au and ^{3}He+Au reactions at incident beam energies of 2.8 and 10 GeV/nucleon, in bins of $\cos\theta$.

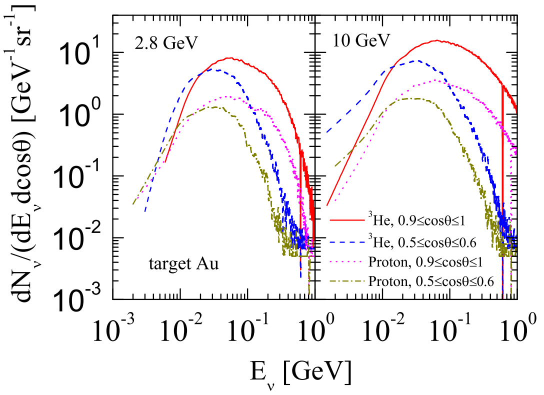

FIG. 11: (Color online) Energy distributions of neutrino production at angles $0.9 < cos\theta < 1$ and $0.5 < cos\theta < 0.6$ from positively charged pion decay in p+Au and ^{3}He+Au reactions at incident beam energies of 2.8 and 10 GeV/nucleon.

neutrinos from low-angle possess more energy than those from high-angles. Note here that neutrino production can also from other channels [33], especially for energetic collisions. For physical experiments relevant to neutrinos, detailed studies of the numbers, the energy spectra as well as the species of emitted neutrinos are very necessary and therefore the simulations related to neutrino production are also become important [33].

In conclusion, proton and ^{3}He induced reactions on ^{197}Au target at beam energies of 2.8, 5, 10 and 16.587 GeV/nucleon are studied in the framework of the Relativistic BUU transport model. It is found that compared with proton induced reactions, ^{3}He induced reactions give larger cross sections of pion production, about 5 times those of the proton induced reactions. And ^{3}He induced reactions are more inclined to low-angle's pion emission. Simulations demonstrate that neutrino emission via positively charged pion decay is also inclined to low-angle emission.

The author G.C. Yong acknowledges B.A. Li for providing the ART model code and Z.W. Lin for providing the new version of the AMPT model. The work is supported by the National Natural Science Foundation of China (10635080, 10875151, 10740420550, 10925526), the Knowledge Innovation Project (KJCX2-EW-N01) of Chinese Academy of Sciences and the one Hundred Person Project (Y101020BR0), the Major State Basic Research Developing Program of China under No. 2007CB815004, and the CAS/SAFEA International Partnership Program for Creative Research Teams (CXTD-J2005-1).

---

[1] L. Wolfenstein, Phys. Rev. **D17**, (1978) 2369.
[2] L. Wolfenstein, Phys. Rev. **D20**, (1979) 2634.
[3] Rabindra N. Mohapatra, Goran Senjanović, Phys. Rev. Lett., **44**, (1980) 912.
[4] Y. Ashie *et al.* [Super-Kamiokande Collaboration], Phys. Rev. Lett. **93**, (2004) 101801.
[5] M. Ambrosio *et al.* [MACRO Collaboration], Phys. Lett. **B566**, (2003) 35.
[6] M. Sanchez *et al.* [Soudan2 Collaboration], Phys. Rev. D **68**, (2003) 113004.
[7] T. Araki *et al.* [KamLAND Collaboration], Phys. Rev. Lett. **94**, (2005) 081801.
[8] M. B. Smy *et al.* [Super-Kamiokande Collaboration], Phys. Rev. D **69**, (2004) 011104.
[9] S. N. Ahmed *et al.* [SNO Collaboration], Phys. Rev. Lett. **92**, (2004) 181301.
[10] E. Aliu, et al. [K2K Collaboration], Phys. Rev. Lett., **94**, (2005) 081802.
[11] S. Abe, et al. [KamLAND Collaboration], Phys. Rev. Lett., **100**, (2008) 221803.
[12] Alessandro Strumia, Francesco Vissani, arXiv:hep-ph/0606054v3
[13] Johann Collot, Harold G. Kirk, Nikolai V. Mokhov, Nuclear Instruments and Methods in Physics Research

A451 (2000) 327.
[14] I. Chemakin, V. Cianciolo, B. A. Cole, R. A. Fernow, A. D. Frawley, et al., Phys. Rev. **C65** (2002) 024904.
[15] I. Chemakin, V. Cianciolo, B. A. Cole, R. C. Fernow, A. D. Frawley, et al., Phys. Rev. **C77** (2008) 015209.
[16] M. Apollonio et al. [HARP Collaboration], Phys. Rev. **C80** (2009) 065204 and references [12-21] therein.
[17] S. Agostinelli *et al.*, GEANT4 Collaboration, Nucl. Instrum. Meth. **A506** (2003) 250.
[18] N.V. Mokhov, S.I. Striganov, "MARS overview", FERMILAB-CONF-07-008-AD, 2007.
[19] K. Gallmeister and U. Mosel, Nucl. Phys. A **826** (2009) 151, arXiv:0901.1770 [hep-ex] (2009).
[20] D.H. Wright *et al.*, AIP Conf. Proc. 896 (2007) 11.
[21] A. Heikkinen *et al.*, arXiv:nucl-th/0306008.
[22] H.W. Bertini, P. Guthrie, Nucl. Phys. **A169** (1971) 670.
[23] G. Folger and H.P. Wellisch, arXiv:nucl-th/0306007.
[24] S.G. Mashnik *et al.*, LANL report LA-UR-05-7321, 2005.
[25] K. Long, Nucl. Phys. **B** (Proc. Suppl.), **154** (2006) 111.
[26] G.F. Bertsch and S. Das Gupta, Phys. Rep., **160**, (1988) 189.
[27] B.A. Li and C.M. Ko, Phys. Rev. **C52**, (1995) 2037.
[28] Zi-Wei Lin, Che Ming Ko, Bao-An Li, Bin Zhang, Subrata Pal, Phys. Rev. **C72**, (2005) 064901.
[29] K. Kubodera, S. Nozawa, Int. J. Mod. Phys, **E3**, (1995) 101.
[30] E. Kolbe, K. Langanke, G. Martínez-Pinedo, P. Vogel, J. Phys, **G29**, (2003) 2569.
[31] T. Leitner and U. Mosel, Phys. Rev. **C82**, (2010) 035503; T. Leitner, L. Alvarez-Ruso, and U. Mosel, Phys. Rev. **C73**, (2006) 065502.
[32] Alexey Yu. Illarionov, Bernd A. Kniehl, and Anatoly V. Kotikov, Phys. Rev. Lett. **106**, (2011) 231802.
[33] A. A. Aguilar-Arevalo, C. E. Anderson, A. O. Bazarko, S. J. Brice, B. C. Brown, et al., Phys. Rev. **D79**, (2009) 072002.